MoViC RASD 2016
13th International Conference on Motion and Vibration Control
12th International Conference on Recent Advances in Structural Dynamics
3-6 July 2016, Southampton

Damage Identification Dependence on Number of Vibration Modes Using Mode Shape Curvature Squares

R Janeliukstis[1], S Rucevskis[1], M Wesolowski[2] and A Chate[1]

[1]Institute of Materials and Structures, Riga Technical University, Riga, Latvia
[2]Department of Structural Mechanics, Faculty of Civil Engineering, Environment and Geodetic Sciences, Koszalin University of Technology, Koszalin, Poland

e - mail: Rims.Janeliukstis_1@rtu.lv

Abstract. In this paper a damage identification algorithm for multiple damage sites based on mode shape curvature square method of vibration mode shapes in aluminium beam is reported. The required mode shape curvature of a healthy structure was obtained via interpolation of mode shape curvature of a damaged structure with Fourier series functions of different orders. Algorithm employed calculations of standardized damage index distributions over beam coordinate. Finite element simulations of proposed methodology involving various artificial noise levels and reduction of mode shape input data points were validated on the damage identification results of experimentally measured mode shapes which were measured using scanning laser vibrometer. Results show that the algorithm is capable of capturing the areas of damage. The term called damage estimate reliability was introduced in terms of likelihood of the chosen approximation function to capture the location of damage.

1. Introduction

Design of modern civil and engineering structures such as automotive and aerospace facilities, stadiums, dams, tunnels, skyscrapers etc., requires higher standards of safety than ever before. Not meeting these objectives may lead to tragic consequences – loss of human lives as well as material losses. To overcome this problem, traditionally rigorous and costly structure inspection procedures took place, however, on top of the already mentioned disadvantages; these procedures were also time-consuming and not always reliable.

A new trend of, so- called, structural health monitoring (SHM) emerged in recent decades. SHM employed the use of various techniques to detect the presence and evolution of damage in structures and therefore maintain their integrity and safety [1]. Out of these techniques the most attention is focused on non-destructive techniques (NDTs). NDTs can be classified into two categories – local and global [2, 3]. In order for local techniques such as X-ray, acoustic or ultrasonic, magnetic field, radiographs, eddy-current and thermal field methods [4], to be usable, the vicinity of damage must be known a priori and this portion of structure must be accessible. These restrictions are avoided through the use of global damage detection methods that employ vibration characteristics of the structure. The underlying idea of global vibration-based damage identification methods is that dynamic characteristics, for example, natural frequencies, mode shapes and damping, of the structure are influenced by the presence of damage [5] in such a way that damage decreases stiffness [2]. This effect is local in nature; therefore the area of damage can be tracked.

Various damage identification methods that are based on mode shapes and their derivatives gained a wide popularity due to ability to assess the structure on a local level [6-11]. Out of these methods a

special attention is paid to mode shape curvature square (MSCS) method, which is based on modal strain energy [12] or modal stiffness [13] comparison between healthy and damaged structure. The need for the modal data of a healthy structure (baseline modal data) is one of the most significant drawbacks of those methods, as baseline modal data is sometimes difficult or even impossible to obtain. This issue is usually solved by employing Gapped Smoothing Techniques to generate a smoothed surface of mode shape curvature, thus simulating a healthy state of the structure [7].

In this paper, MSCS method was employed in damage identification for aluminium beam containing two sites of mill-cut damage. The location of damage was assessed without the baseline modal parameters. This was accomplished using interpolation of mode shape curvature of a damaged structure with Fourier series functions of different orders, thus yielding a mode shape curvature of a healthy structure. Damage was characterized with a damage index (DI) and its later standardization based on statistical hypothesis approach, leading to a standardized damage index (SDI). This damage identification algorithm (DIA) was carried out on numerically simulated vibrational mode shapes, corrupted with various levels of artificial noise and reduced by integer numbers to study the effects of sensor density. These two effects were studied simultaneously for different combinations of mode sums involved in the computation. The effectiveness of damage identification algorithm was assessed through the damage estimate reliability (DER); measuring (in percentage) how well the area of damage was located. Results from numerical simulation were validated on an identical algorithm for operational deflection shapes, measured experimentally with a scanning laser vibrometer and an excitation was performed with a PZT element.

2. Materials and methods

2.1 Damage identification algorithm (DIA)

Most of the mode shape curvature damage detection methods require the baseline data of the healthy structure for inspection of the change in the modal parameters due to damage. However, in most cases this data is not available.

In this paper, an interpolation technique with a Fourier series approximation was applied on a MSC data of the damaged structure, generating smooth mode shape curvatures that are estimates of the healthy structure. The Fourier series is a sum of sine and cosine functions that describes a periodic signal. The trigonometric Fourier series form is

$$\kappa(x) = a_0 + \sum_{i=1}^{g} a_i \cdot \cos(g\omega x) + b_i \cdot \sin(g\omega x) \quad (1)$$

where a_0 models a constant (intercept) term in the data, ω is the fundamental frequency of the signal, g is the number of terms (harmonics) in the series [14].

In this study, mode shape curvature data was approximated with Fourier series functions of orders 1 to 8 ($1 \leq g \leq 8$). The obtained coefficient values a_0, a_i, b_i and ω were used to reconstruct the approximation of MSC data using equation (1). The damage index is defined as the absolute difference between the measured curvature of the damaged structure and reconstruction of mode shape curvature approximation with Fourier series representing the healthy structure. The maximum value indicates the location of damage. For the mode at grid point i

$$DI_{i\ MSCS}^{n} = \left| \left(\frac{\partial^2 w^n}{\partial x^2} \right)_i^2 - \left(\kappa_x^n \right)_i^2 \right| \quad (2)$$

where w^n is measured transverse displacement of the structure, κ_x^n is reconstruction of Fourier series approximation of MSC data in x direction, n is a mode number. It must be noted that the value of the calculated MSC as well as approximation reconstruction at grid point were normalized with respect to the largest value of each component. The MSC were calculated from the mode shapes by the central difference approximation at grid point i as:

$$\left(\frac{\partial^2 w^n}{\partial x^2}\right)_i = \frac{\left(w_{i+1}^n - 2w_i^n + w_{i-1}^n\right)}{h^2} \quad (3)$$

where h is the distance between two successive nodes or measured points.

In practice, however, experimentally measured operational deflection shapes are always corrupted by measurement noise at some extent. This may even lead to false peaks in damage index profiles, misleading the data interpreter. To overcome this problem, it is proposed to calculate a summarized damage index, which is defined as the average summation of damage indices for all modes N, normalized with respect to the largest value of each mode

$$DI_i = \frac{1}{N} \cdot \sum_{n=1}^{N} \frac{DI_i^n}{DI_{i,\max}^n} \quad (4)$$

According to [15, 16], the damage indices, determined for each element, are then standardized

$$SDI_i = \frac{DI_i - \mu_{DI}}{\sigma_{DI}} \quad (5)$$

where μ_{DI} and σ_{DI} are mean value and standard deviation of damage indices in equation 4, respectively. After the standardization a concept of statistical hypothesis testing was applied to classify damaged and healthy elements and to localize damage depending on the pre-defined damage threshold value: choose H_0 (element i of the structure is healthy) if $SDI_i < C_r$ or choose H_1 (element i of the structure is damaged) if $SDI_i \geq C_r$, where C_r is a threshold value. Typical values of C_r, widely used in literature are 1.28, 2 and 3 for 90 %, 95 % and 99 % confidence levels for the presence of damage.

To quantify the reliability of Fourier series functions to identify damage location, a new parameter, called „*damage estimate reliability*" (DER) was introduced and calculated as follows:

- The whole interval along the axis of the beam (x axis) was split into 2 parts:
  - the 1st part (a) was the one which does not contain damage, namely
    0 mm < x < 450 mm, 500 mm < x < 750 mm and 800 mm < x < 1250 mm (part a);
  - the 2nd part (b), containing damage, was 450 mm < x < 500 mm and 750 mm < x < 800 mm.
- In each of these parts standardized damage indices (SDIs) from equation (5) of a respective approximation function were summed and divided by the number of data points in this particular interval, giving average amplitude of SDI ($\overline{SDI_i}$).
- DER is equal to average SDI in the area of damage (part b) divided by average SDI in all parts combined. It is expressed in percentage as:

$$DER_i = \frac{\overline{SDI_i}(b)}{\overline{SDI_i}(a) + \overline{SDI_i}(b)} \times 100\% \quad (6)$$

2.2 Numerical simulations

The validation of proposed damage identification algorithm was performed by numerical modal analysis based on finite element method (FEM). It was conducted by using the commercial software ANSYS. An aluminium beam with two mill-cut damage sites was considered. Geometrical configuration of the beam is shown in figure 1. The first and second mill-cut damage sites with a depth of 2 mm and width of 50 mm were introduced at a distance of 450 mm and 750 mm from one edge of the beam, respectively. FE model of the beam consists of 2D beam elements. Each node has 3 degrees of freedom, namely translations along the X and Y axes and rotation along the Z axis. The beam was constructed by means of 148 equal length elements (i = 149 nodes). The elastic material properties are taken as follows: Young's modulus E = 69 GPa, Poisson's ratio ν = 0.31, and the mass density ρ = 2708 kg/m^3. The damage is modelled by reducing the flexural stiffness of the selected elements, which is achieved by decreasing the thickness of elements in the damaged region of the beam. In total, 11 modal frequencies and corresponding mode shapes were calculated.

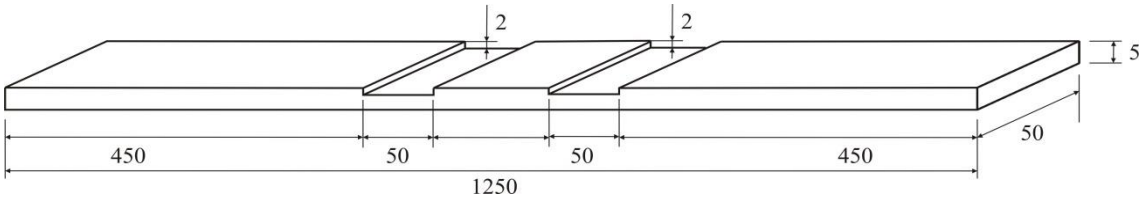

Figure 1. Geometry and dimensions of tested aluminium beams.

In order to compare the sensitivity of the DIA to noisy experimental data, a uniformly distributed random noise was added to the numerically simulated mode shapes

$$w_n'^i = w_n^i \cdot (1 + \delta \cdot (2r - 1)) \quad (7)$$

where prime indicates noisy mode shapes, δ is a level of random noise and r are uniformly distributed random values in the range (0, 1).

It is often not possible to equip the structure with a dense grid of sensors. Therefore an additional study was conducted where numerical mode shape data was divided by integer numbers p = 1, 2, 3, 4, 5, and 6, leading to mode shape vectors of length 149, 75, 50, 38, 30 and 25.

2.3 Influence of number of mode shapes on DIA results

The contribution of different numbers of modes in damage localization was tested. As soon as the appropriate approximation function was chosen, the following calculations took place:

- SDI and respective DER values for different numbers of vibration modes were calculated according to equation (6) for all p values at each of noise level δ = 0 %, 0.1 %, 0.3 %, 0.54 %, 1 %, 2 % and 4 %, forming a DER matrix, where columns correspond to p values and rows – to noise levels. Thus 10 DER matrices of dimensions 7x6 were obtained for the cases of sum of DI values over all 11 modes, 10, 9, 8, 7, 6, 5, 4, 3 and lastly over 2 modes.
- DER values at δ = 0 % (DER(δ = 0 %)) were considered and upper and lower limit values (DERUL and DERLL, respectively), corresponding to DER(δ = 0 %) ± δ, were calculated as follows:

$$DERUL = DER(\delta = 0\%) + DER(\delta = 0\%) \times \delta \quad (8)$$

$$DERLL = DER(\delta = 0\%) - DER(\delta = 0\%) \times \delta \quad (9)$$

- In order to test, whether DER values fall within the interval DERUL-DERLL, a new parameter, named Outlier Damage Estimate Reliability (ODER) was calculated for all levels of noise according to expression

$$ODER(\%) = \begin{array}{l} IF(DER(\delta) > DERUL) \\ \qquad DO(|\, DERUL - DER(\delta)\,|), \\ ELSE(DER(\delta) - DERLL) \end{array} \quad (10)$$

2.4 Experiment

Resonant frequencies of the test beam were measured by a POLYTEC PSV-400-B scanning laser vibrometer (SLV). General experiment set-up consisted of a PSV-I-400 LR optical scanning head equipped with a highly sensitivity vibrometer sensor (OFV-505), OFV-5000 controller, PSV-E-400 junction box, a Bruel & Kjaer type 2732 amplifier, and a computer system with a data acquisition board and PSV software (figure 2). The system requires defining the geometry of the object and setting up a scanning grid. To match the finite element model, 126 equally spaced scanning points were distributed to cover a beam along its length. In order to simulate clamped-clamped (two ends fixed) boundary conditions experimentally, two vices were used to fix the ends of the beam (10 mm from both sides) with the clamped torque equal to 20 Nm. The beam was then excited by a periodic

input chirp signal generated by the internal generator with a 1600 Hz bandwidth through a piezoelectric actuator (PZT). After the measurement is performed at one point, the vibrometer automatically moves the laser beam to another point of the scan grid, measures the response using the Doppler principle, and validates the measurement with the signal-to-noise ratio. The procedure is repeated until all scan points have been measured. The resonance frequencies and corresponding operational deflection shapes are obtained by taking the fast Fourier transform of the response signal.

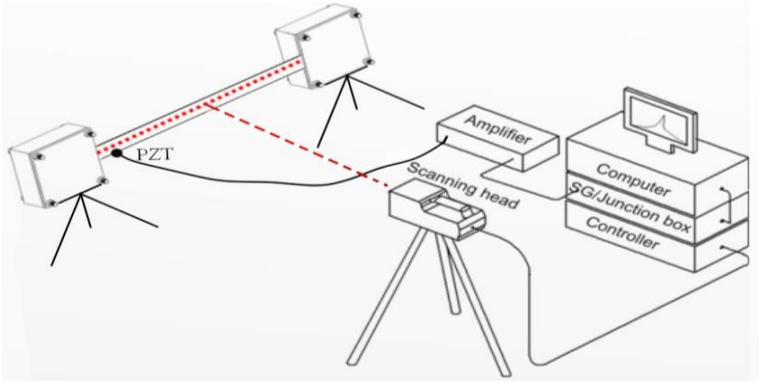

Figure 2. Experimental set-up.

3. Results and discussion

3.1 Numerical simulation results

DER analysis of SDI was performed for each of the Fourier fitting functions, labeled F1 through F8. The respective DER values for damage index sum over all modes at p =1 are shown in table 1.

Table 1. FEM DER values for Fourier series fitting functions, sum of all modes at p = 1.

Fitting function	F1	F2	F3	F4	F5	F6	F7	F8
DER (%)	94.53	94.75	94.83	94.56	94.24	94.03	93.87	93.86

As one can see, the best fitting function turned out to be F3 with a DER = 94.83 %. Afterwards, DER analysis was performed at each individual mode using F3 (refer to table 2).

Table 2. FEM DER values for F3 function for each of individual modes at p = 1.

Mode	2nd	3rd	4th	5th	6th	7th	8th	9th	10th	11th	13th
DER (%)	94.92	93.81	94.76	93.35	93.68	92.88	92.16	94.76	95.09	94.27	93.88

The 10th mode showed the best results in terms of DER, yielding 95.09 %. The following analysis was conducted to test how various combinations of mode sums affect the reliability of damage identification. The sum of damage indices from 6 modes resulted in best DER value, namely, 94.99 % (table 3).

Table 3. FEM DER values for F3 function at different mode sum combinations at p = 1.

Mode sum	2	3	4	5	6	7	8	9	10
DER (%)	94.88	94.86	94.69	94.69	94.99	94.81	94.87	94.86	94.88

Plots of standardized damage index distributions over the coordinate of the beam SDI(x) are shown in figure 3 and figure 4. These plots were calculated for 2 cases - for damage index sum over all modes and for the particular mode that yielded the best DER value.

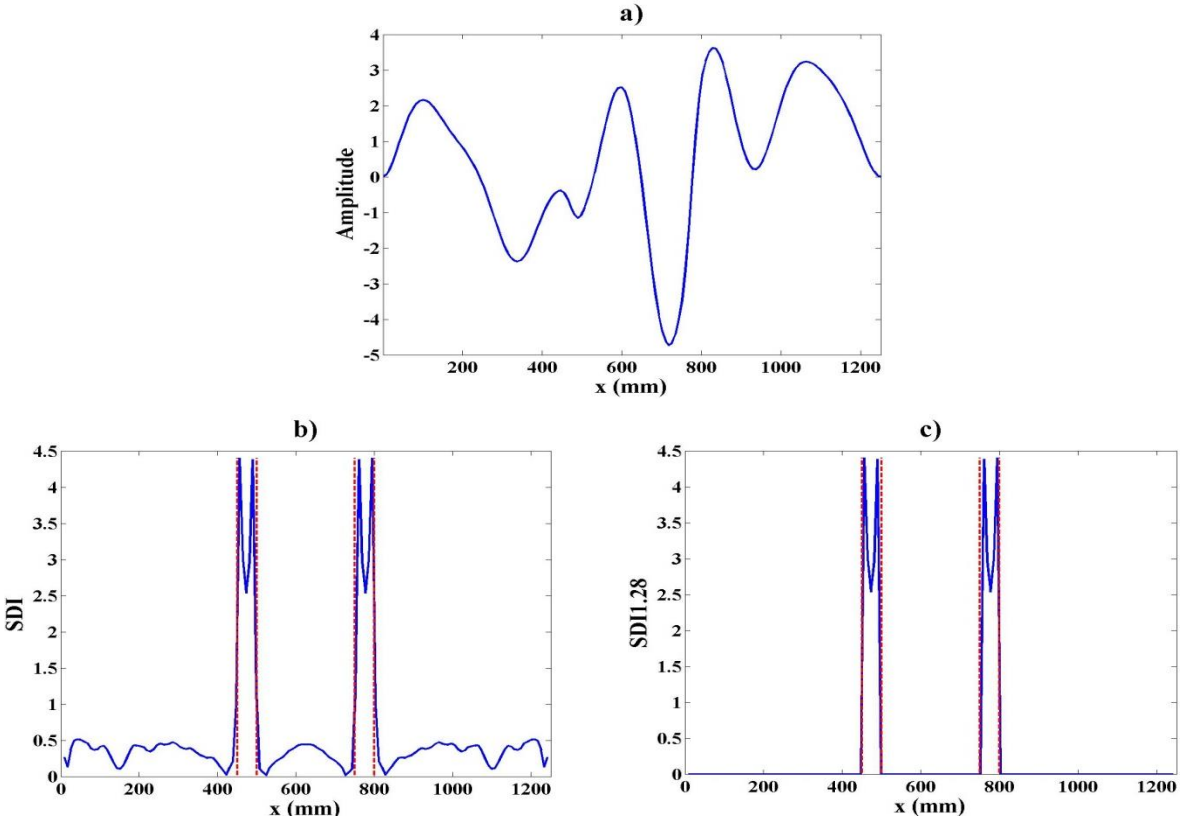

Figure 3. SDI(x) for sum of damage indices over all modes: *a*) mode shape sum, *b*) SDI, *c*) $SDI_{1.28}$.

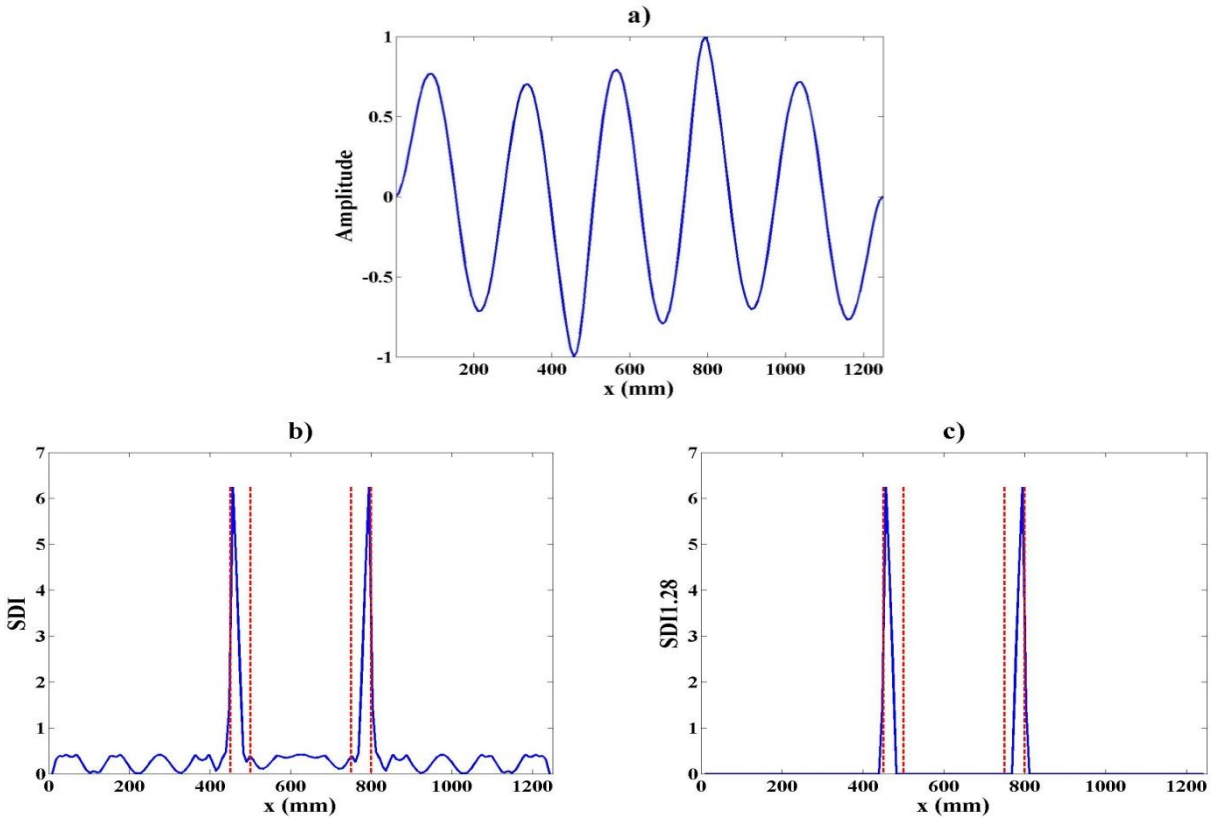

Figure 4. SDI(x) for best mode (mode 10): *a*) mode shape, *b*) SDI, *c*) $SDI_{1.28}$.

A thresholded SDI distribution is obtained from the original SDI(x) plot by setting to zero those SDI values that do not exceed the value of the threshold. This level of threshold is selected such, that a 100 % DER value is achieved. In all cases it turned out to be 1.28, therefore plots of $SDI_{1.28}$ are shown. The respective mode shapes are also plotted. It can be seen, that in both cases DIA managed to capture the location of damage as highest peaks appear between 2 red vertical lines (depicting the predetermined area of damage).

DER matrices were calculated for sums of standardized damage indices over different combinations of modes and are shown in figure 5.

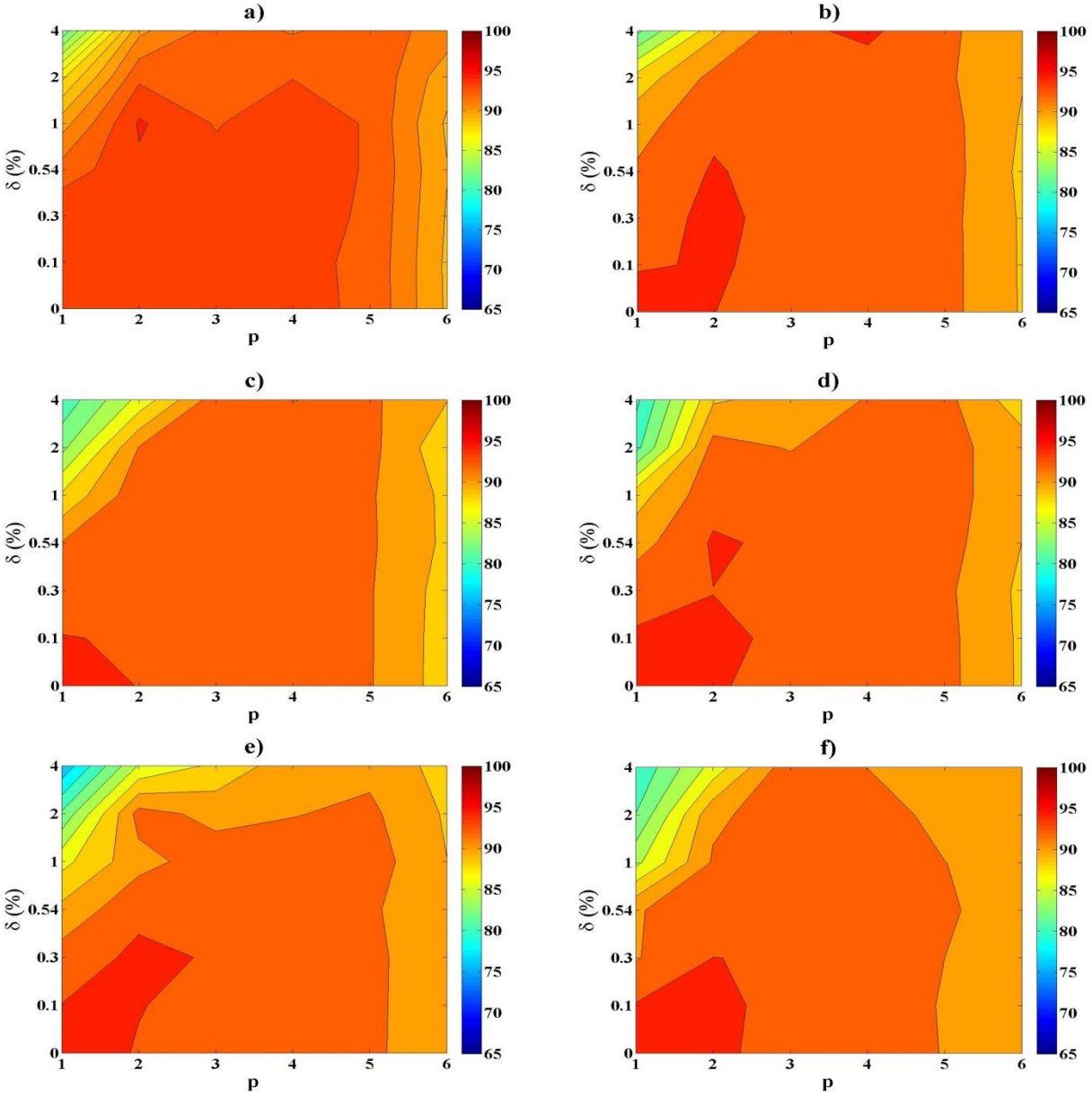

Figure 5. DER matrices for DI sums over different numbers of modes:
a) 11 modes, *b*) 10 modes, *c*) 9 modes, *d*) 8 modes, *e*) 7 modes, *f*) 6 modes.

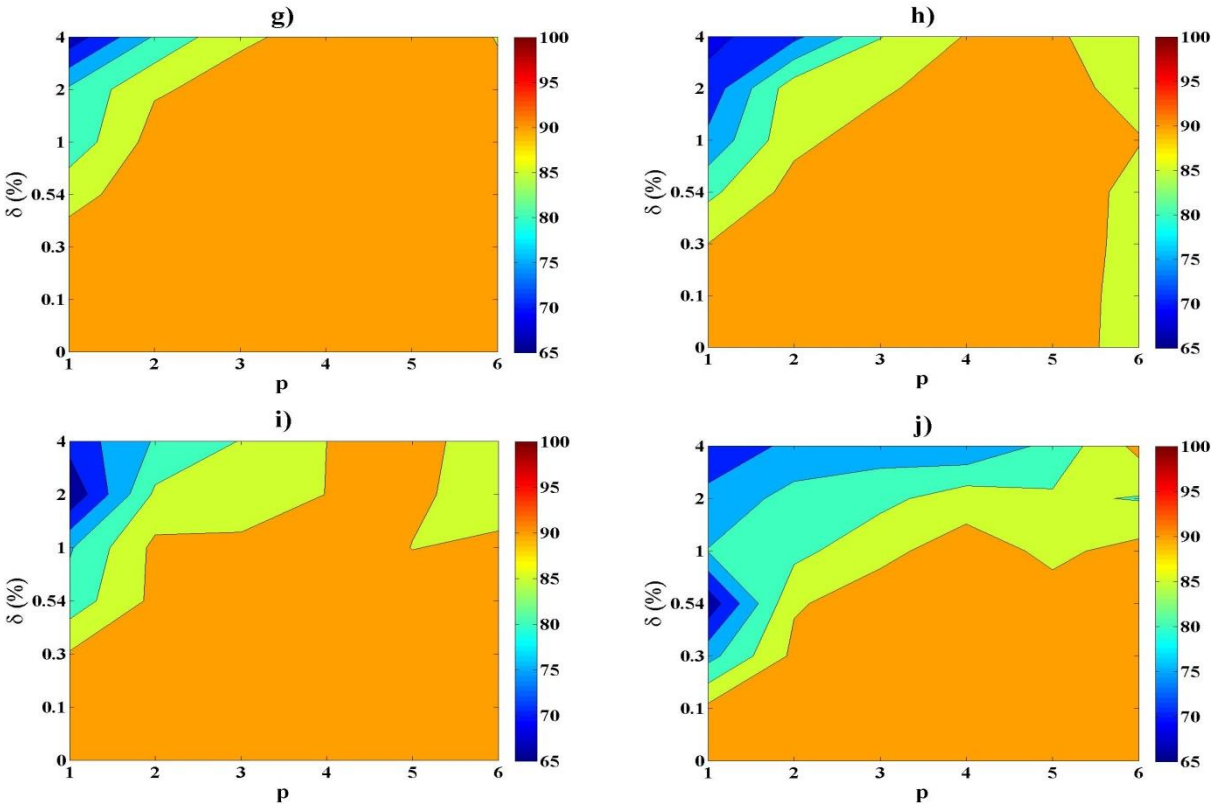

Figure 5. DER matrices for DI sums over different numbers of modes:
g) 5 modes, *h*) 4 modes *i*) 3 modes and *j*) 2 modes.

For damage index sums over higher modes (from 1:6 to 1:11) noise affects only cases with largest density of sensors (p = 1), while for the case of 2 modes the noise contamination occurs at all sensor densities and overall DER values are lower.

ODER values for the respective combinations of mode sums are shown in figure 7. ODER values increase with the increasing value of p, indicating if structure is equipped with fewer sensors, it is also less susceptible to noise. This holds true for all combinations of mode sums, nevertheless, as number of modes is increased, ODER values are becoming more positive (rising) for a fixed density of sensors. At damage index sums starting from 7 modes and higher ODER values become nearly constant at about p = 3, while if DI sums over fewer modes are involved in the computation, smallest fluctuations of ODER occur at higher p values. Overall, cases with higher numbers of modes are less distorted by noise and reach constant ODER values at smaller p.

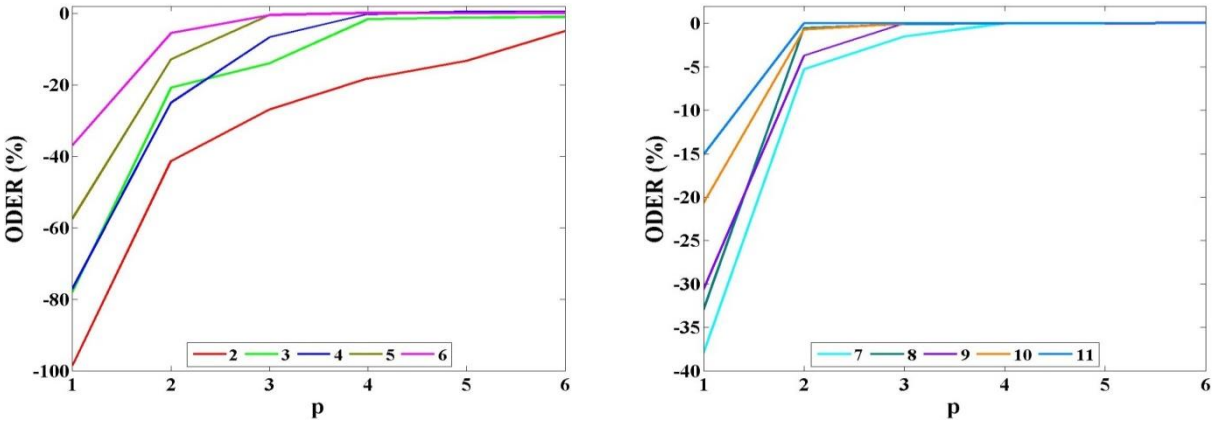

Figure 6. ODER vs sensor density for DI sums over different numbers of modes.

3.2 Experimental results

DER values for SDI for F1to F8 for damage index sum over all modes at $p = 1$ are shown in table 4.

Table 4. Experimental DER values for Fourier series fitting functions, sum of all modes at $p = 1$.

Fitting function	F1	F2	F3	F4	F5	F6	F7	F8
DER (%)	94.10	94.22	94.32	94.08	93.85	93.50	93.36	93.05

Similarly to numerical simulations, the best fitting function turned out to be F3 with a DER value of 94.32 %. The respective DER analysis at each individual mode can be seen in table 5. The mode for SDI with the best DER value (95.30 %) is 9th mode.

Table 5. Experimental DER values for F3 function at each of individual modes at $p = 1$.

Mode	2nd	3rd	4th	5th	6th	7th	8th	9th	10th	11th	12th
DER (%)	77.61	87.82	94.44	90.70	93.66	93.88	90.96	95.30	93.21	92.76	93.96

Table 6 shows the DER values for DI sum over different combinations of modes for F3. As the damage index summation is performed over more modes, the DER value also tends to increase. The highest value of DER, corresponding to sum of DI over 9 modes, is 93.80 %.

Table 6. Experimental DER values for F3 function at different mode sum combinations at $p = 1$.

Mode sum	2	3	4	5	6	7	8	9	10
DER (%)	82.65	91.18	91.76	92.47	92.80	92.84	93.39	93.80	93.59

SDI distributions for the same two cases were calculated for experiment as well. The contribution of standardized damage index from all modes together with a respective mode shape plot is shown in figure 7, while the respective SDI contribution from best mode is shown in figure 8.

As one can see, in both cases the highest peaks of SDI are located right between the red vertical lines (in the zone of damage) and SDI threshold of 1.28 ($SDI_{1.28}$) is enough to reach 100 % of DER.

The results regarding analysis of how sensor density affects DER values for damage index sum over different combinations of modes can be seen in figure 9. The lowest DER corresponds to sum of 2 modes at $p = 1$ and, as p increases, DER value also increases, reaching maxima at $p = 3$. At $p > 3$, DER decreases a little. As for DI sum over 3 modes till DI sum over 6 modes there are only slight decreases of DER value as p increases. The same trend can be observed for DI sum over higher number of modes (from 1:7 till 1:11). It can be concluded that highest DER values of standardized damage index correspond to $p = 2$ throughout the majority of mode sum combinations and that there is no significant gain to damage identification algorithm in terms of DER as the number of modes is increased.

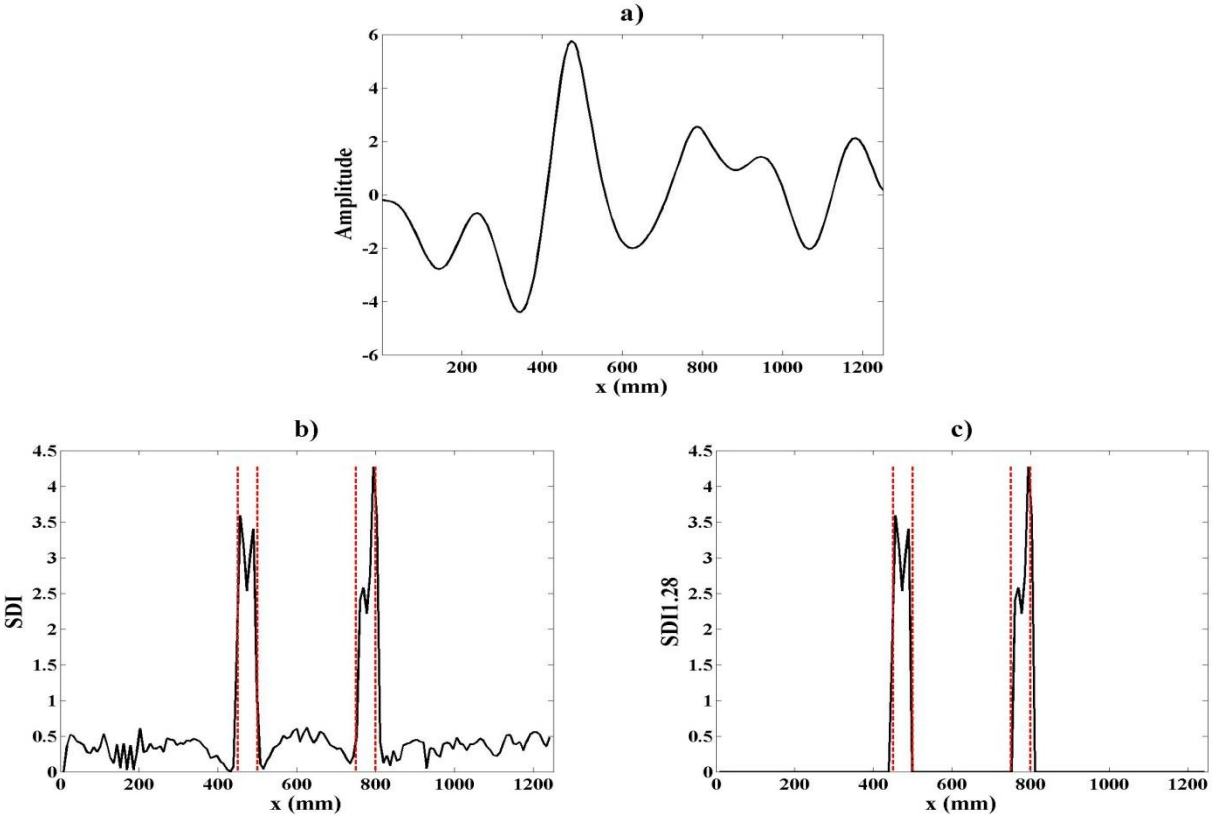

Figure 7. SDI(x) for sum of damage indices over all modes: *a*) mode shape sum, *b*) SDI, *c*) $SDI_{1.28}$.

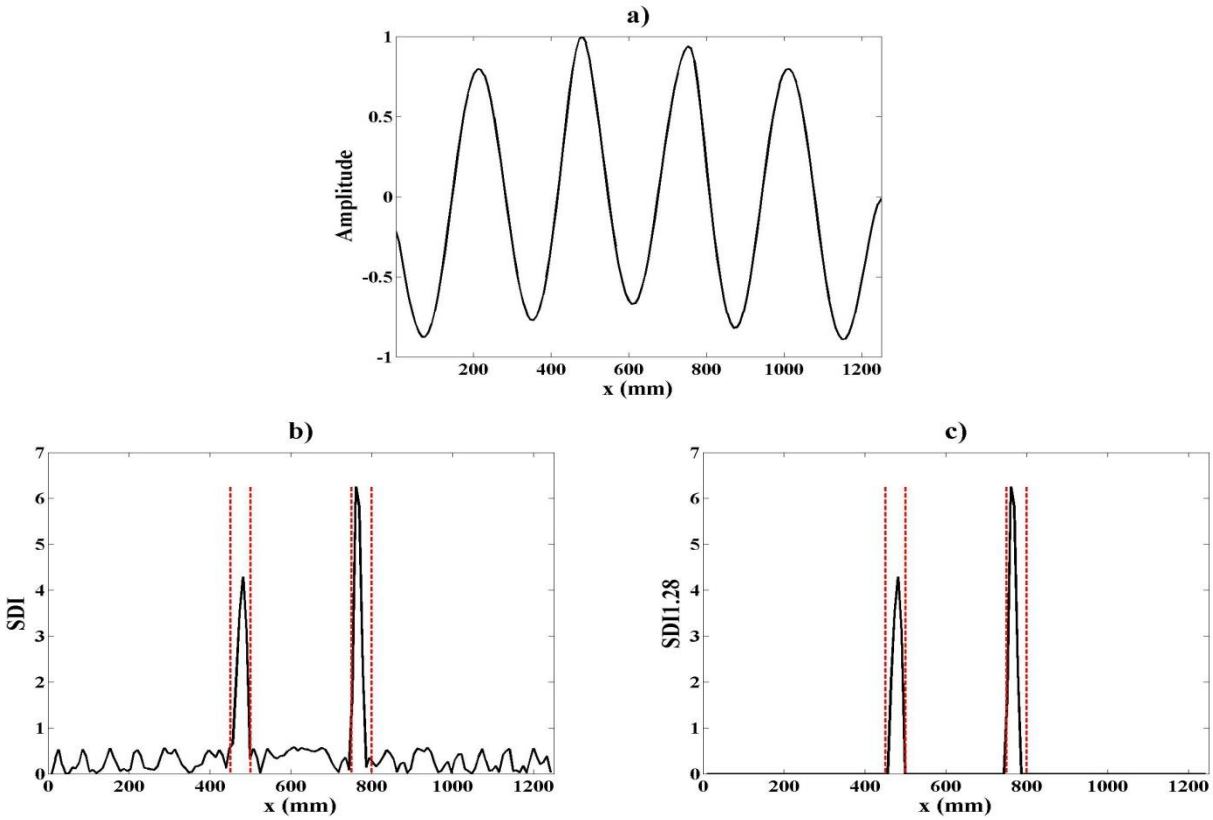

Figure 8. SDI(x) for best mode (mode 9): *a*) mode shape, *b*) SDI, *c*) $SDI_{1.28}$.

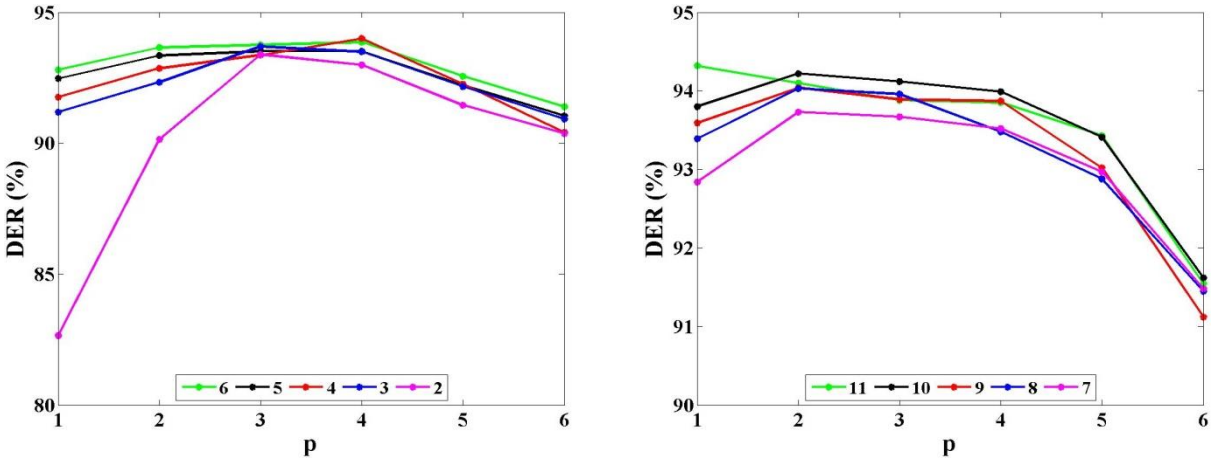

Figure 9. DER vs sensor density for DI sums over different numbers of modes.

4. Conclusions

The damage identification based on mode shape curvature square method was successfully demonstrated on an aluminium beam containing 2 sites of mill-cut damage.

Damage identification algorithm was tested in numerical simulations in cases with damage index sums over different numbers of modes, each for different noise levels and sensor densities, yielding matrices, where likelihood of damage indication for each of these cases was expressed in percentage through damage estimate reliability parameter. This methodology was validated on an experimentally measured operational deflection shape data. For numerical simulation as well as for experimental cases Fourier series function of order 3 yielded the best damage identification results in terms of damage estimate reliability value for standardized damage index. For largest sensor density these values were 94.83 % and 94.32 %, respectively. In order to test the influence of noise on standardized damage index at each of mode shape vector lengths, Outlier damage estimate reliability values were calculated. Results suggest that without the presence of noise there is no problem for damage identification algorithm to localize the area of damage at all sensor densities and combinations of damage index sums. While the addition of noise deteriorates the reliability of standardized damage index to detect damage, this effect was observed mainly for a denser sensor grid. For damage index sums over modes 1:2 to 1:5, the adverse effect of high level noise was observed also for a coarser sensor grid.

In general, for numerical simulations as well as for experimental cases, the following observation was made – the more modes are considered for summing of damage indices, the better damage identification results are obtained. As indicated by the experimental results, highest DER values for most of the mode number combinations corresponded at moderate sensor density.

Acknowledgements

The research leading to these results has received the funding from Latvia State Research Programme under grant agreement "Innovative Materials and Smart Technologies for Environmental Safety, IMATEH".

References

[1] Montanari L, Basu B, Spagnoli A and Broderick B M 2015 A padding method to reduce edge effects for enhanced damage identification using wavelet analysis *Mech. Syst. Signal Pr.* **52-53** 264–27.

[2] Fan W and Qiao P 2009 A 2-D continuous wavelet transform of mode shape data for damage detection of plate structures *Int. J. Solids Struct.* **46** 4379–95.

[3] Alamdari M M, Li J and Samali B 2015 Damage identification using 2-D discrete wavelet transform on extended operational mode shapes *Arch. Civ. Mech. Eng.***15** 698–10.

[4] Doebling S W, Farrar C R, Prime M B and Shevitz D W 1996 Damage Identification and Health

Monitoring of Structural and Mechanical Systems from Changes in Their Vibration Characteristics: A Literature Review *Los Alamos National Laboratory Report (LA-13070-MS)*.
[5] Hong J C, Kim Y Y, Lee H C and Lee Y W 2002 Damage detection using the Lipschitz exponent estimated by the wavelet transform: applications to vibration modes of a beam *Int. J. Solids Struct.* **39** 1803–16.
[6] Ulriksen M D and Damkilde L 2016 Structural damage localization by outlier analysis of signal-processed mode shapes – Analytical and experimental validation *Mech. Syst. Signal Pr.* **68-69** 1-14.
[7] Qiao P, Lu K, Lestari W and Wang J 2007 Curvature mode shape-based damage detection in composite laminated plates *Compos. Struct.* **80** 409–28.
[8] Rucevskis S, Sumbatyan M A, Akishin P and Chate A 2015 Tikhonov's regularization approach in mode shape curvature analysis applied to damage detection *Mech. Res. Commun.* **65** 9–16.
[9] Lestari W and Qiao P 2005 Damage detection of fiber-reinforced polymer honeycomb sandwich beams *Compos. Struct.* **67** 365–73.
[10] Chandrashekhar M and Ganguli R 2009 Damage assessment of structures with uncertainty by using mode-shape curvatures and fuzzy logic *J. Sound Vib.* **326** 939–57.
[11] Dawaria V B and Vesmawala G R 2013 Modal curvature and modal flexibility methods for honeycomb damage identification in reinforced concrete beams *Procedia Eng.* **51** 119 – 24.
[12] Dessi D and Camerlengo G 2015 Damage identification techniques via modal curvature analysis: Overview and comparison *Mech. Syst. Signal Pr.* **52-53** 181–205.
[13] Kim J T and Stubbs N 2002 Improved damage identification method based on modal information *J. Sound Vib.* **252**(2) 223-38.
[14] Matlab R2014a: http://se.mathworks.com/help/curvefit/fourier.html.
[15] Bayissaa W L, Haritosa N and Thelandersson S 2008 Vibration-based structural damage identification using wavelet transform *Mech. Syst. Signal Pr.* **22** 1194–15.
[16] Kim J-T, Ryu Y-S, Cho H-M and Stubbs N 2003 Damage identification in beam-type structures: frequency-based method vs mode-shape-based method *Eng. Struct.* **25** 57–67.